Journal of Nuclear Materials 619 (2026) 156267

Contents lists available at ScienceDirect

Journal of Nuclear Materials

journal homepage: www.elsevier.com/locate/jnucmat

Deuterium retention and erosion resistance of low-pressure plasma sprayed tungsten coatings

G. Schmidtmann [a,b,*], A. Litnovsky [a], A. Kreter [a], M. Rasinski [a], S. Möller [b], A. Houben [a], J.W. Coenen [a,c], R. Vaßen [b], S. Brezinsek [a], Ch. Linsmeier [a], O. Guillon [b], G. Mauer [b]

[a] Forschungszentrum Jülich GmbH, Institute of Fusion Energy and Nuclear Waste Management – Plasma Physics (IFN-1), Jülich, 52425, Germany
[b] Forschungszentrum Jülich GmbH, Institute of Energy Materials and Devices - Materials Synthesis and Processing (IMD-2), Jülich, 52425, Germany
[c] Department of Nuclear Engineering & Engineering Physics, University of Wisconsin -Madison, Madison, 53706, United States of America

ARTICLE INFO

Keywords:
Low-pressure plasma spraying
Plasma-facing material
Plasma exposure experiments
Tungsten
Sputtering yield
Deuterium retention
In-situ/ex-situ repair

ABSTRACT

Low-pressure plasma-sprayed (LPPS) tungsten coatings of 300 μm thickness were produced with optimized production parameters to demonstrate the feasibility of the process as a repair technique for eroded or damaged plasma-facing components. The samples were, in two separate experiments, exposed to Neon (Ne) and Deuterium (D) plasma to investigate the sputtering resistance and the deuterium retention, and compare the performance to similarly exposed reference bulk tungsten samples. After applying a total fluence of $2{\cdot}10^{24}$ ions/m^{2}s Ne ions with an ion impact energy of 100 eV at a sample temperature of 60 °C, the LPPS coatings showed a 0% to 20% higher sputtering yield than the similarly exposed reference bulk tungsten, indicating a slightly decreased performance. The deuterium plasma was characterized by 73 eV ions, and the exposure was run at a sample temperature of 250 °C, until the plasma fluence was $3{\cdot}10^{25}$ ions/m^{2}s. The deuterium retention, which was evaluated using nuclear reaction analysis as well as thermal desorption spectroscopy, demonstrated an enhanced performance of the LPPS coatings, indicated by a lower total D inventory potentially by outgassing. In addition, the spectra indicated a D desorption at lower temperatures than that for pure bulk tungsten for the LPPS coatings and a significant impact of the LPPS process parameters on the grain structure and, therefore, the retention performance.

1. Introduction

Tungsten (W) as the main plasma-facing material (PFM) candidate in future fusion devices such as DEMO, exhibits advantageous thermal properties, a relatively short decay time when activated, a low sputtering yield by plasma, high creep resistance, and low hydrogen retention and permeation. Despite all these positive characteristics, tungsten is not immune to defects, including crack formation, melt damage or erosion accompanied by re-deposition due to impurities. Erosion of the first wall material will lead to decreased surface thickness of the armor layer, resulting in a reduced lifetime of the device. Defects or changes in material properties caused by hydrogen retention or neutron-induced activation can even lead to maintenance periods and must therefore be understood well and kept at a low rate.

The light fuel elements deuterium (D) and tritium (T) interact with the PFM and can be trapped in vacancies and voids of the material, causing property changes such as embrittlement [1] and in addition, at high damage rate impacts the tritium cycle process. [2].

Low-pressure plasma spraying (LPPS) is a method of addressing and repairing potential damages and erosion by depositing dense layers of pure tungsten on the underlying materials. This process can rapidly and efficiently restore the thickness of the wall to the necessary level. LPPS is characterized by its capacity to produce high-quality coatings of materials with high melting points. The process parameters can be modified in order to achieve high densities and deposition efficiency, which is accompanied by low oxidation rates due to the protective Ar atmosphere.

In the present work, the samples were exposed to (Ne) plasma to evaluate the sputtering resistance of the LPPS produced coatings. In a second experiment, a deuterium (D) plasma was applied to examine possible deuterium retention and accumulation in the coatings. A variety of analysis techniques were utilized to investigate the distinct impact of the plasma on different characteristics prior to and after the plasma exposure.

* Corresponding author.
E-mail address: g.schmidtmann@fz-juelich.de (G. Schmidtmann).

https://doi.org/10.1016/j.jnucmat.2025.156267
Received 1 August 2025; Received in revised form 23 September 2025; Accepted 29 October 2025

Available online 5 November 2025

2. Experimental setup and analysis methods

2.1. Sample preparation

In plasma exposure experiments described in this paper utilized samples produced by LPPS on two substrate materials: tungsten (W) and Eurofer97 steel (referred to as Eurofer in the subsequent text), a ferritic martensitic steel with low activation, developed especially for fusion applications (hereafter in sample names and plots referred to as E) [3–5]. The tungsten substrate material is a pure tungsten manufactured by Plansee Holding AG and will be further referred to as W in plots and graphs. Tungsten represents the main candidate for PFM and armor of the underlying materials [6,7] while Eurofer is a promising candidate as structural material in future fusion devices such as DEMO [8].

The LPPS process is a widely known thermal spray process applied for high-melting metals and ceramics, using a plasma jet and fine spray powders. In the context of this work, the process was characterized by a 60 mbar surrounding vacuum/light argon (Ar) atmosphere, which acts as a suppressant for unwanted interactions. The process was distinguished by a relatively low powder feed rate, which facilitated enhanced energy transfer from the plasma flume to the particles. Furthermore, a high plasma enthalpy is facilitated through a high hydrogen (H) content in the plasma gas mixture [9]. The spray gun was mounted on a computerized numerical control (CNC)-system and moved over the substrates mounted in the sample holder. The Y-directional meander distance between the single passes in X-direction was 4 mm. Due to the austenitization temperature during the production of Eurofer steel, it was necessary to pause the coating process after each pass over for one minute, while on tungsten substrates a continuous coating process was applied [4,3]. In addition, the velocity of the nozzle passing over the Eurofer substrate was doubled to 440 mm/s, to minimize the heat impact of the substrate, resulting in a corresponding doubling of the number of pass overs to achieve a comparable coating thickness. The applied spray process parameters have been optimized in previous studies and can be found in [10].

All coatings were produced at the Jülich Thermal Spray Center (JTC) [11] using a F4-VB spray gun by Oerlikon. The objective was to create coatings of high density with a thickness of approx. 500 µm in order to conduct the plasma exposure experiments on a realistic thickness for future fusion applications.

The surface of all coatings was polished with a final alkaline oxide polishing suspension (SiO_2) with a particle size of 0.05 µm resulting in a surface roughness R_a of approx. 0.1 µm. Prior to the exposure experiments, the samples were cleaned by ultrasonic bath and outgassed in a vacuum furnace at 550 °C for 3 hours. In consequence and for a better comparability, all samples were prepared similar. Additional information on the sample preparation can be found in [10].

2.2. Analysis methods

Various methods were employed to evaluate the samples pre- and post-plasma exposure. Scanning electron microscope (SEM) images were taken using DSM 982 manufactured by Zeiss. Additional SEM images were taken using a dual-beam scanning electron microscope with ion beam (SEM/FIB - Zeiss Crossbeam 540) manufactured by Zeiss. To evaluate the local erosion, craters with orthogonal cuts were created using the focused-ion-beam (FIB) technique prior to the exposure, as commonly applied for erosion measurements [12,13]. Furthermore, the surface recession allows to calculate a mass loss taking into account the density of the coating. The total weight loss due to erosion is determined by means of weighing the samples before and after exposure experiments with a Sartorius MSA225P microbalance with a readability of d = 0.01 mg.

In order to measure and to compare the surface roughness of the samples before and after plasma exposure, the CyberScan CT350T confocal white light sensor system produced by cyberTECHNOLOGIES GmbH with a resolution of 0.035 µm was employed. The value R_a represents the mean value of absolute surface height values of seven linear measurement lines in x- and y-direction, each containing 50 measurement points. The area considered corresponded to the entire sample, excluding one millimetre from the edges on all sides.

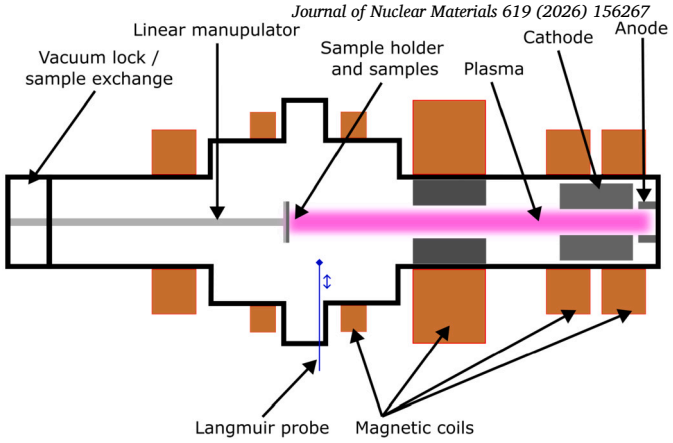

Fig. 1. Schematic setup of the linear plasma device PSI-2 along with plasma, sample holder, linear manipulator, plasma.

Nuclear Reaction Analysis (NRA), using a 2950 ± 20 keV ^{3}He ion beam, was applied to investigate the D-retention in a single 1 x 1 mm^2 spot analysis. The amount of D is quantified using the D(^{3}He,p)^{4}He reaction [14], the end-station, described in [15], and simNRA 7.03 [16]. The interaction of ^{3}He with the D in the samples results in the emission of a proton, which is measured by an applied Si-detector. This non-destructive method allows to evaluate the trapped D in the sample up to a depth of approx. 4 µm. Furthermore, NRA allows to detect other elements such as carbon using ^{12}C(^{3}He,p)^{14}Ne [17,18], nitrogen ^{14}N(^{3}He,1+2)^{16}O [19] and oxygen ^{16}O(^{3}He,p)^{18}F [20]

All measurement spots were located in the very center of the sample and resulted in a depth profile from the surface to 4 µm depth. In addition, the carbon (C), oxygen (O), and, for the surface layer, the nitrogen (N) content of the samples can be displayed.

In the final investigation step of the analysis, the samples were measured using thermal desorption spectroscopy (TDS). The exposed samples were heated in an oven with a heating ramp of 10 K per minute and degassed. The thermally desorbed gas species were measured using two quadrupole mass spectrometers (QMS). The desorbing D and HD molecules allow an evaluation of the fuel retention of the exposed samples in dependence on the temperature. A ramp-and-hold degassing ramp with a heating ramp up to 600 °C, a 60 minutes holding time was applied for the coatings on Eurofer substrate, whereas the coatings on tungsten substrate were exposed to a second heating ramp until 1000 °C accompanied by a second 60 minuts holding time.

In all cases, a reference sample has been measured alongside the main sample. The quantitative analysis of the reference sample facilitates a comparison between the performance of the LPPS-produced coatings and that of the bulk tungsten.

2.3. Plasma exposure experiments

2.3.1. General arrangement

Plasma exposure experiments were carried out in the linear plasma device PSI-2 [21] using two different plasmas, neon (Ne) plasma and deuterium (D) plasma. A schematic of PSI-2 can be found in Fig. 1, described with anode, cathode and most relevant setups. More details and information on the PSI-2 can be found in the literature [21,22].

Each exposure was carried out for four samples, accompanied by one reference sample from forged bulk tungsten. A list of all exposed samples can be found in Table 1 including plasma species and production process. The samples were mounted in a hollow profile (compare Fig. 2

Table 1
Samples with exposure species carried out in the experiments. E and W represent the substrate materials tungsten and Eurofer, PSI the experiment, H is one of two low-pressure plasma spraying production parameter (more details in [10]).

Sample	Plasma species
E_PSI_H_1	Ne
E_PSI_H_2	Ne
W_PSI_H_1	Ne
W_PSI_H_2	Ne
Ref_W_1	Ne
E_PSI_H_3	D
E_PSI_H_4	D
W_PSI_H_5	D
W_PSI_H_6	D
Ref_W_2	D

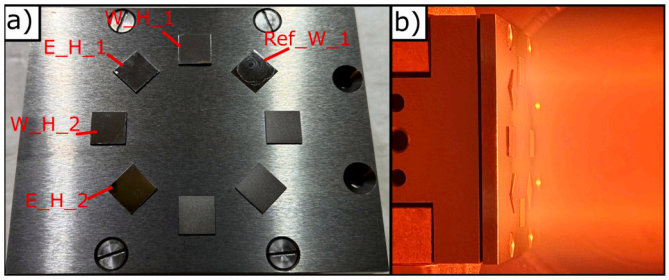

Fig. 2. Setup of the Ne plasma exposure experiments with a) sample holder with four mounted samples, one reference sample Ref_W_1 and three placeholder. Image b) displays the Ne-plasma exposure of W-coatings in the PSI-2.

Table 2
Experimental Ne plasma parameters for the linear plasma device PSI-2.

Plasma	Ion energy (eV)	Ion flux (ions/m^{2}s)	Ion fluence (ions/m^2)	T_{sample} (°C)
Neon (Ne)	100	$5.2{\cdot}10^{20}$	$2.0{\cdot}10^{24}$	65

a) in a mask of molybdenum. No cooling was applied to the mask or the samples. The sample temperature was measured using infrared thermography and compared to the data obtained from thermocouples attached to the backside of the sample holder.

2.3.2. Sputtering resistance

To investigate the sputtering resistance of the coatings, the first PSI-2 campaign was carried out using singly ionized Ne plasma with energies of approx. 100 eV controlled by the target biasing of approx. -120 V. The experimental plasma details such as ion energy and sample temperature are listed in Table 2, the sample setup inside the mask can be found in the Fig. 2 a, an image of the exposure with plasma is shown in image 2 b.

2.3.3. Deuterium retention

The investigation of the retention and accumulation of the hydrogen isotopes in the plasma-sprayed tungsten coatings involved a second set of four samples and one additional reference sample. These samples were exposed to D plasma. The experimental conditions, such as sample distribution and preparation, were kept similar to those of the Ne exposure (compare section 2.3.2) with the exception of the plasma parameters and exposure time, listed in Table 3. The temperature of the samples was monitored using thermal couples attached to the backside of the sample holder.

Table 3
Experimental D plasma parameters for the linear plasma device PSI-2.

Plasma	Ion energy (eV)	Ion flux (ions/m^{2}s)	Ion fluence (ions/m^2)	T_{sample} (°C)
Deuterium (D)	73	$3.8 \cdot 10^{21}$	$3{\cdot}10^{25}$	250

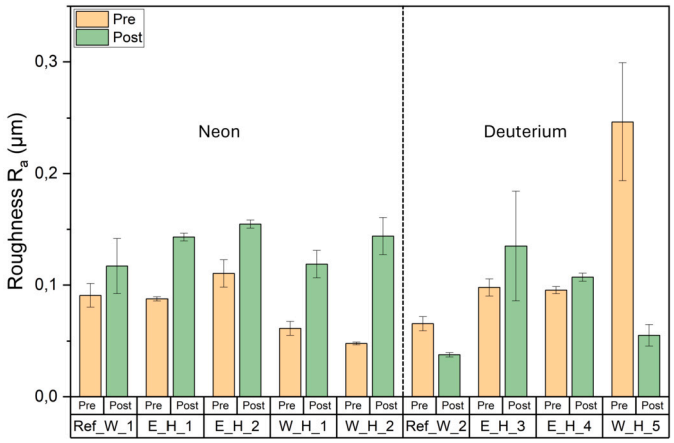

Fig. 3. Sample roughness R_a taken from the surface using the CyberScan. In the interest of optimizing the available space, the term "PSI" has been omitted in the description of all LPPS samples illustrated in the figure.

3. Results and discussion

3.1. Surface modifications by D and Ne plasma

The scanning electron microscope images taken from the sample surface pre- and post-exposure exhibit unusual melting-like formations on an area of approx. 1.5 mm x 1.5 mm of sample E_PSI_H_3 after D plasma exposure, resulting in a noticeable large error. EDX mappings and cross-section images using FIB-cuts of the area did not reveal the presence of impurities or other oxide contamination, nor did they reveal any unusual grain structure changes.

The surface roughness R_a taken pre- and post-exposure is shown in Fig. 3. The samples exposed to Ne plasma exhibit an increased surface roughness after exposure. The LPPS coatings exhibit a larger increase in roughness than the reference sample, for which, in addition, the error bars are overlapping, indicating a non-significant discrepancy.

Varying results in the surface roughness R_a were found for the D-exposed samples. Some samples indicate a smoothing effect, whereas sample E_PSI_H_4 has a non-significant increased surface roughness after exposure. While W_PSI_H_5 pre-exposure can be seen as an outlier, which may result from an irregularity during the polishing preparation or production procedure, the reference sample Ref_W_2 exhibits a decrease in surface roughness after D exposure. The results do not indicate a trend, whether the D exposure increases or decreases the surface roughness.

The melting-like structure on sample E_PSI_H_3 was not evident for other samples in this campaign and can therefore only be explained by defects or impurities implemented inside or on the surface of the sample during the production process or sample preparation. An interaction of the impurities such as oxides, which were not evident after the exposure experiments, can not be excluded. Other surface changes, such as the increased surface roughness R_a after Ne exposure, can be attributable to the distinct sputtering processes which can be enhanced by initial porosity and grain orientation. The influence of the porosity on the physical sputtering yield and its increased surface roughness due to preferential

Table 4
Measured surface recession of the samples after Ne plasma exposure experiment, including calculated mass loss assuming 99.7% density of the LPPS samples within the recession area. Furthermore, measured mass loss of the samples after Ne plasma exposure experiment. Measured using a Sartorius MSA225P microbalance with a readability of d = 0.01 mg with no repetition.

Sample	Ref_W_1	E_H_1	E_H_2	W_H_1	W_H_2
Surface recession (µm)	1.95 ± 0.03	2.21 ± 0.01	2.21 ± 0.12	2.2 ± 0.04	1.95 ± 0.001
Mass loss calc. (mg)	3.73 ± 0.06	4.23 ± 0.02	4.23 ± 0.23	4.2 ± 0.08	3.73 ± 0.002
Mass loss meas. (mg)	3.29	4.00	3.78	4.12	4.03

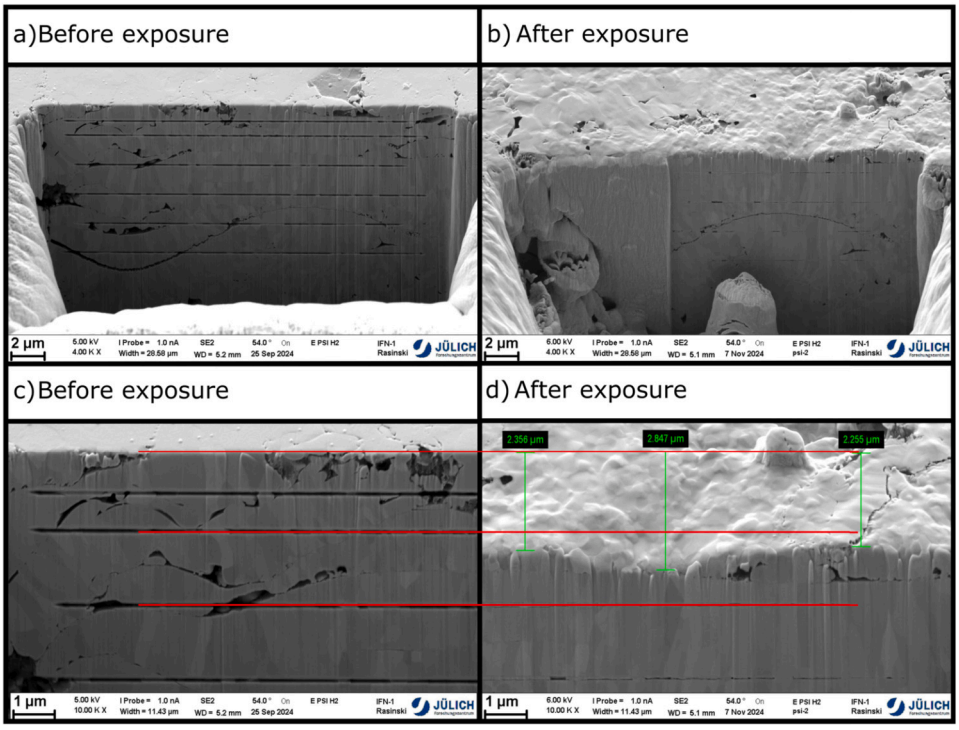

Fig. 4. FIB crater and marker of sample E_PSI_H_2 before and after Ne plasma exposure in PSI-2 device.

sputtering and grain orientation is generally known as well as described and simulated [23–25]. Given the low magnetic field of PSI-2 (0.1 T), rising roughness resulting from re-deposition can be neglected here.

The varying R_a results for D exposure are rarely induced by the sputtering of the hydrogen species. The ion energy of 73 eV is clearly below the sputtering threshold energy of the target tungsten. However, smaller initial displacements induced by the bombardment of D ions or of impurities such as a small 0.1% fraction of oxygen [26,27] in the plasma may have occurred. This effect can smoothen the surface of some samples and roughen it for others, resulting from the initial roughness or grain structure.

Changes in the surface morphology can be induced by D retention, such as blisters, which were found on all D-exposed samples. Furthermore, accumulations of D in the deeper, underlying regions, as found for higher fluence in [28] lead to increased surface roughness while other work found a nearly constant surface roughness or only small increases after D-exposure [29] or argon (Ar) seeded D plasma [30]. While the blister formation has been visible for all samples and therefore could have locally increased the surface roughness, any impact of impurities in the plasma on the smoothing of the surface can not be concluded here. In total the presented results do not confirm any impact of the blistering on the surface roughness R_a

From the data presented in this work, it is not possible to deduce whether there is a clear increase or decrease in roughness for the samples exposed to D at low fluence in this experiment. This finding supports the hypothesis that due to the low ion energy, only a minor impact on the roughness is induced by D ions, and that this impact is almost not significant.

3.2. Sputtering resistance

The sputtering resistance of the samples was evaluated using the mass loss induced by the Ne plasma, listed in Table 4. The results were compared to the surface recession taken from the FIB markers in the center of the samples (example shown in image 4). The recession allows the mass loss to be calculated taking density and material properties into account, as shown in Table 4. The mass loss calculated from the surface recession is largely consistent with the measured mass loss.

The measured mass loss of the LPPS coatings exceeds the reference sample by 14% to 25% while the surface recession is 0% to 13% larger than that of the reference sample. In no case did the LPPS coatings exhibit a sputtering yield below that of the reference sample.

The theoretically calculated mass loss by Eckstein [31] on a flat surface for 100 eV Ne ions, assuming a normal incidence for all impacting particles, results in a sputtering yield of approximately $3.15{\cdot}10^{-2}$ atoms/ion. This results in a total mass loss of 2.5 mg for the applied ion fluence, assuming 10% Ne^{2+}. These values deviate more significantly from the measured values.

The impact of grinding the edges of the samples to fit them into the mask on the mass loss can be effectively excluded, as the measured mass loss and recession mass loss are in similar ranges. The results obtained are thus found to be accurate.

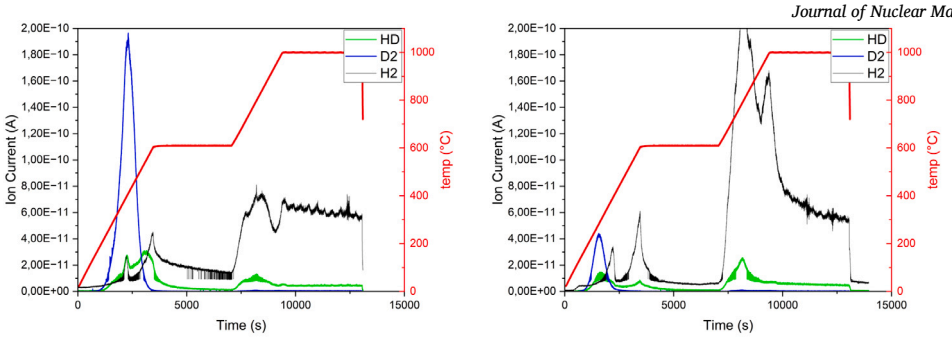

Fig. 5. Desorption spectra of the molecular D_2, HD and H_2 as ion current in ampere (A) and temperature (°C) of the sample a) reference sample Ref_W_2 and b) W_PSI_H_5 against the time.

Binary Collision Approximation (BCA) calculations which can base on Eckstein values [31] do not take include re-deposition of sputtered tungsten. Consequently, the bare calculated yield according BCA and perfectly polishes surfaces generally falls below the measured values, which is not evident in this study. Additional ERO simulations [32] are needed to validate the findings.

In addition, a negative impact of increasing porosity on the sputtering yield was found by Mao et al. for different porosity in W_fW tungsten fiber-reinforced tungsten matrix materials [33]. Despite the slightly higher porosity of LPPS coatings compared to the reference sample, this effect is not visible in this work. Instead, the LPPS coatings exhibit a higher sputtering yield compared to the reference bulk tungsten.

Other impurities in the Ne plasma may have contributed to the erosion, as also to be seen in other experiments [33,34]. The surface roughness (R_a) resulting from porosity and varying grain structure in the coatings has been shown to generally decrease the sputtering yield [35]. However, in certain specific cases, depending on the incident angle of the ion onto the substrate target, an increase in yield may be observed [36]. Induced by a more complex relationship between material, ion energy, and incident angle, Cupak et al. suggest that in some cases, the surface roughness or, more specific here, the porosity resulting from a specific incident angle of the projectile ion onto the target substrate can induce a higher sputtering yield [36]. The roughness of the LPPS coatings is primarily attributed to the comparatively deep pores with extensive smooth areas between them. This non-homogeneous distributed surface roughness due to 0.3% of partly deep pores in the LPPS coatings may have exerted a substantial influence on the sputtering yield.

The substantial disparity in grain size or grain orientation [37,13], between the LPPS coatings with small grains and the reference tungsten sample with large grains can also impact the sputtering yield. While the influence of grain structure on sputtering yield is well known, grain size correlations known from sputtering targets [38] do not appear to have any or only a small influence here [39].

Overall, the sputtering yield of the LPPS coatings remains in an acceptable range compared to the bulk tungsten. The increased sputtering results from the finer grain structure containing unmolten particles, accompanied by pores or voids. The discrepancy to the theoretical value could be linked to the 100 eV ions energy, which, according to the Eckstein values, is located on an edge of the sputtering yield for Ne projectile on W target [31].

3.3. Deuterium retention

Fig. 5 illustrates selected plots of the measured TDS analysis as ion current against time for the species D_2, HD and H_2. The bulk tungsten reference sample Ref_W_2 in Fig. 5 a shows a significantly higher D_2 peak compared to the plasma-sprayed sample in Fig. 5 b. However, the hydrogen peak (H_2), as illustrated in Fig. 5 b, exhibits a substantially

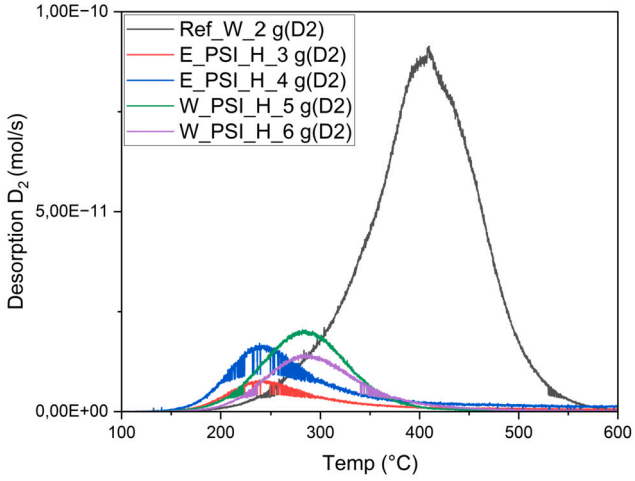

Fig. 6. Desorption spectra of D_2 desorption in mol/s for all D-plasma exposed samples against the desorption temperature.

higher value in comparison to the reference sample. For both cases, the primary D_2 peak is located within the first temperature ramp of the experiment, starting at approx. 200 °C to 250 °C and is decreasing again before the ramp reaches T = 600 °C. An additional minor D_2 peak is located at 600 s or approx. 700 °C. Peaks of the HD signal are always linked to peaks of the H_2 signal. As a result of the low degassing temperature of 550 °C, desorption peaks beyond a temperature of 600 °C can not clearly be dedicated to the loading by the PSI-2 plasma. Taking this, the rather small D_2 peak beyond 600 °C shown in Fig. 5 and the consistent correlation between the H_2 peaks and the HD peaks, which could indicate falsely measured HD signal, into account, the main focus will be set on a final desorption temperature of T = 600 °C.

Therefore, Fig. 6 illustrates the desorption of D_2 for all samples as a function of the temperature up to 600 °C. The curve for the reference sample rises from approx. 200 °C, whereas the D_2 desorption of the LPPS samples begins at lower temperatures of approx. 150 °C. The desorption temperature of 200 °C exhibited by the reference sample Ref_W_2 is almost consistent with the exposure temperature, a phenomenon that is systematically observed for bulk tungsten.

The temperature at which the Eurofer substrate samples exhibit the D peak is approximately 240 °C, while that of the tungsten samples is approximately 280 °C. The peak of the reference sample is at 420 °C and is significantly higher. Besides the main desorption peak, a small shoulder at slightly higher temperatures can be detected for several samples. The reference sample exhibits the shoulder peak at approx. 480 °C.

The spectra of reference sample Ref_W_2 shown in Fig. 6 show a standard spectrum for the desorption of D_2 from dense tungsten. The

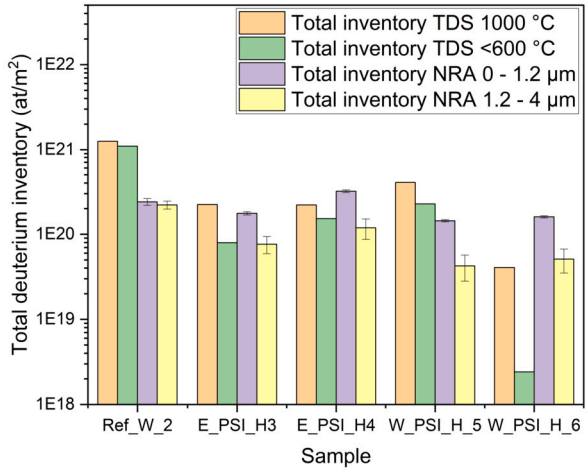

Fig. 7. The total D inventory of all samples measured by NRA with depth profile and TDS for two desorption temperatures. The TDS inventory < 600 °C includes all desorbed values until the TDS temperature reached 600 °C while the inventory 1000 °C takes all desorbed values into account.

second peak, shouldering at approximately 480 °C, which can also be seen in some of the LPPS coatings, is known from the literature [40,41].

The D diffusion and trapping is typically associated with the density of traps, which are characterized by defects in the lattice, grain boundaries, and voids within the sample. In the context of plasma-sprayed coatings, the desorption of D at lower temperatures has been previously detected by Golubeva et al. [42]. However, the dominant factor was identified as the enhanced porosity of the coatings in comparison to the reference tungsten, which can be neglected as a factor in this work. Plasma-sprayed W coatings with no open porosity have been found to exhibit an increased hydrogen retention [43,44] compared to bulk tungsten, more dense and homogeneous tungsten materials. In contrast to the results obtained previously, the results presented in this work indicate a lower D retention and therefore an increased performance with respect to the D retention, and permit alternative interpretations. In contrast to the NRA results, which show only minor differences between the reference sample and the plasma-sprayed samples, the TDS measurements clearly indicate a superior performance of the plasma-sprayed coatings compared to the reference sample.

The integrated D_2 desorption up to 600 °C and 1000 °C shown in Fig. 7 indicates slightly lower desorption until 600 °C than the total desorption to 1000 °C. Solely for sample W_PSI_H_6 a significant difference can be observed. The NRA results reveal higher D in surface near regions compared to the deeper region. The NRA values are found to be largely in good agreement, while for the reference sample Ref_W_2 being significantly lower than the measured TDS values. This frequently documented phenomenon may be linked to a deeper diffusion of the D into the reference tungsten, beyond the depth resolution limitations of the NRA measurements but can not be validated here [45–49]. However, the reference sample exhibits the expected TDS and NRA values given the level of deuterium exposure [50].

A pathway formation to the surface of the samples initiated by an increased porosity value supports a fast D release and suppresses further diffusion and accumulation into the bulk [51,52] and consequently, elevated D retention values were observed in the reference sample with minimal porosity in the literature [53,43]. Nevertheless, an enhanced surface near porosity of the LPPS coatings, resulting in an early release of D can be neglected as the coatings exhibit a porosity of approx. 0.3%.

A more likely explanation for the superior performance of the LPPS coatings with 0.3% porosity compared to the qualitatively dense bulk tungsten is the corresponding grain structure, which can be described as columnar and is shown in a previous publication in more detail [10]. As described earlier, the majority of deuterium retention takes place at the grain defects and boundaries in tungsten samples [54–56]. Grain boundaries can not only act as deuterium traps but also as deuterium channels towards the surface [57,58]. In most cases, the grain structure of LPPS produced samples can be described as a columnar grain structure in the direction of the surface of the sample which therefore can enhance the escaping channels for trapped hydrogen species. This can also explain the earlier described desorption of D at lower temperatures which was determined for the LPPS coatings. Accumulation of hydrogen weakens the bonding between the grains and can initiate cracks along those [58]. Larger amounts of hydrogen can be trapped at those areas but also be released more easily.

The elevated nozzle speed over the substrate during the production of the coatings using LPPS resulted in a generally smaller grain size and therefore can result in an earlier trapping and release of D [42,59,9]. The influence of a higher porosity leading to a lower desorption temperature is well known and described in [52] but can be seen as negligible here due to almost similar porosity of reference and LPPS samples.

Among the LPPS coatings and different substrate materials, no differences in porosity can be determined. Rather, the coatings are characterized by different grain size. The coatings produced on the W substrate demonstrate a maximal feret diameter of 2.5 ± 1.8 µm while those on the Eurofer substrate only exhibit 1.8 ± 1.0 µm. A smaller grain size and, as a consequence, an increased number of grain boundaries can precipitate desorption at lower temperatures. Since the reference sample contains solely large grains compared to the LPPS coatings with rather small grains, earlier desorption of the species can occur for the LPPS coatings. [59]

4. Conclusion

Low-pressure plasma-sprayed tungsten coatings on tungsten and Eurofer substrates were exposed to Ne and D plasma in two individual experiments in the linear plasma device PSI-2 to investigate their plasma performance with respect to sputtering resistance and D retention. Results from mass loss and surface recession demonstrate an increased sputtering yield for the LPPS coatings compared to the bulk tungsten reference sample and theoretical values. This increase can be attributed to the smaller grain size of the LPPS coatings as well as the roughness of the surface. This not only illustrates the major impact of the grain size on the D retention but also highlights the impact of the production factors, such as the raster speed and substrate temperature, on the performance.

The TDS retention results contrast sharply with previous findings published in the literature, which showed that the plasma-sprayed coatings retained more deuterium than bulk tungsten. These publications explain the higher retention by the increased porosity of the coatings and the accumulation of hydrogen in these defects [42,60,44], but also by the microstructure of the LPPS coatings [59,44]. Since the coatings presented in this work do not exhibit increased porosity, the lower retention must be explained solely by the columnar grain structure, whereby the grain boundaries function as desorption channels. This paper demonstrates that LPPS facilitates the deposition of dense tungsten coatings with reduced D retention. Consequently, its performance is comparable to that of bulk tungsten, and it can be considered a viable repair method for eroded PFCs.

CRediT authorship contribution statement

G. Schmidtmann: Writing – original draft, Visualization, Validation, Project administration, Methodology, Investigation, Formal analysis, Data curation. **A. Litnovsky:** Writing – review & editing, Supervision, Project administration, Methodology, Investigation, Funding acquisition, Conceptualization. **A. Kreter:** Resources, Investigation, Formal analysis. **M. Rasinski:** Writing – review & editing, Resources, Formal analysis. **S. Möller:** Writing – review & editing, Investigation, Formal analysis. **A. Houben:** Resources, Formal analysis. **J.W. Coenen:** Supervision, Resources. **R. Vaßen:** Supervision, Resources. **S. Brezinsek:** Su-

pervision, Resources. **Ch. Linsmeier:** Resources. **O. Guillon:** Resources. **G. Mauer:** Writing – review & editing, Supervision, Project administration, Funding acquisition, Conceptualization.

Declaration of generative AI use

Statement: During the preparation of this work the author(s) used Grammarly (by Grammarly Inc.) in order to increase readability. After using this tool/service, the author(s) reviewed and edited the content as needed and take(s) full responsibility for the content of the published article.

Declaration of competing interest

The authors declare the following financial interests/personal relationships which may be considered as potential competing interests: Gunnar Schmidtmann reports a relationship with European Consortium for the Development of Fusion Energy that includes: funding grants. If there are other authors, they declare that they have no known competing financial interests or personal relationships that could have appeared to influence the work reported in this paper.

Acknowledgements

The authors want to thank the technical staff at IFN-2 and IMD-2, in particular Johannes Spelthann, Karl-Heinz Rauwald, Noah Richter, Ulf Knoche, Giulian Katzenstein and Fabienne Weitz for their help and technical assistance in preparing the experiments.

This work has been carried out within the framework of the EUROfusion Consortium, funded by the European Union via the Euratom Research and Training Programme (Grant Agreement No 101052200 — EUROfusion). Views and opinions expressed are however those of the author(s) only and do not necessarily reflect those of the European Union or the European Commission. Neither the European Union nor the European Commission can be held responsible for them.

Data availability

Data will be made available on request.

References

[1] H. Khodja, C. Brosset, N. Bernier, Deuterium inventory in plasma facing materials by means of nra: a microbeam probe approach, Nucl. Instrum. Methods Phys. Res., Sect. B, Beam Interact. Mater. Atoms 266 (8) (2008) 1425–1429, https://doi.org/10.1016/j.nimb.2007.11.027.

[2] T. Loarer, C. Brosset, J. Bucalossi, P. Coad, G. Esser, J. Hogan, J. Likonen, M. Mayer, P. Morgan, V. Philipps, V. Rohde, J. Roth, M. Rubel, E. Tsitrone, A. Widdowson, Gas balance and fuel retention in fusion devices, Nucl. Fusion 47 (9) (2007) 1112–1120, https://doi.org/10.1088/0029-5515/47/9/007.

[3] M. Rieth, M. Schirra, A. Falkenstein, P. Graf, S. Heger, H. Kempe, R. Lindau, H. Zimmermann, Eurofer 97. Tensile, charpy, creep and structural tests, https://doi.org/10.5445/IR/270055720.

[4] X. Chen, A. Bhattacharyaa, K.D. Linton, Y. Yamamoto, M.A. Sokolov, L.N. Clowers, Y. Katoh, Mechanical properties and microstructure characterization of unirradiated eurofer-97 steel variants for the eurofusion project, Fusion Eng. Des. 146 (2019), https://doi.org/10.2172/1471901.

[5] E. Gaganidze, F. Gillemot, I. Szenthe, M. Gorley, M. Rieth, E. Diegele, Development of eurofer97 database and material property handbook, Fusion Eng. Des. 135 (2018) 9–14, https://doi.org/10.1016/j.fusengdes.2018.06.027.

[6] I. Catanzaro, P. Arena, S. Basile, G. Bongiovì, P. Chiovaro, A. Del Nevo, P.A. Di Maio, R. Forte, I.A. Maione, E. Vallone, Structural assessment of the eu-demo wcll central outboard blanket segment under normal and off-normal operating conditions, Fusion Eng. Des. 167 (2021) 112350, https://doi.org/10.1016/j.fusengdes.2021.112350.

[7] J. Boscary, G. Ehrke, P. Frosi, P. Junghanns, B. Končar, B. Mendelevitch, D. Naujoks, R. Neu, M. Richou, L. Selan, J. Tretter, Z. Wang, J.H. You, K. Zhang, Conceptual design of the next generation of w7-x divertor w-target elements, Fusion Eng. Des. 192 (2023) 113629, https://doi.org/10.1016/j.fusengdes.2023.113629.

[8] P. Arena, G. Bongiovì, I. Catanzaro, C. Ciurluini, A. Collaku, A. Del Nevo, P.A. Di Maio, M. D'Onorio, F. Giannetti, V. Imbriani, P. Maccari, L. Melchiorri, F. Moro, R. Mozzillo, A. Noce, L. Savoldi, S. Siriano, A. Tassone, M. Utili, Design and integration of the eu-demo water-cooled lead lithium breeding blanket, Energies 16 (4) (2023) 2069, https://doi.org/10.3390/en16042069.

[9] R.B. Heimann, Plasma Spray Coating: Principles and Applications, 2nd edition, Wiley-VCH, Weinheim, 2008.

[10] G. Schmidtmann, Y.J. Sohn, A. Litnovsky, M. Rasinski, R. Vaßen, J.W. Coenen, S. Brezinsek, C. Linsmeier, O. Guillon, G. Mauer, Optimizing plasma spraying process parameters for tungsten coatings used in fusion reactors, J. Therm. Spray Technol. (2025), https://doi.org/10.1007/s11666-025-02034-z.

[11] R. Vassen, Jülich thermal spray center (jtsc) - a new research and innovation infrastructure of forschungszentrum Jülich, Ceram. Forum Int. 97 (2020) 22, https://juser.fz-juelich.de/record/872685.

[12] J. Peng, A. Litnovsky, A. Kreter, Y. Krasikov, M. Rasinski, U. Breuer, J.L. Chen, Sputtering tests of single crystal molybdenum and rhodium mirrors at high ion fluence for in situ plasma cleaning of first mirrors in iter, Fusion Eng. Des. 128 (2018) 107–112, https://doi.org/10.1016/j.fusengdes.2018.01.061.

[13] M. Rasiński, S. Brezinsek, A. Kreter, T. Dittmar, K. Krieger, M. Balden, P. de Marne, R. Dux, M. Faitsch, A. Hakola, J. Likonen, E. Tsitrone, V. Rohde, Fib line marking as a tool for local erosion/deposition/fuzz formation measurements in asdex upgrade during the He campaign, Nucl. Mater. Energy 37 (2023) 101539, https://doi.org/10.1016/j.nme.2023.101539.

[14] M. Nocente, G. Gorini, J. Källne, M. Tardocchi, Cross section of the d + 3 he → α + p reaction of relevance for fusion plasma applications, Nucl. Fusion 50 (5) (2010) 055001, https://doi.org/10.1088/0029-5515/50/5/055001.

[15] S. Möller, D. Höschen, S. Kurth, G. Esser, A. Hiller, C. Scholtysik, C. Dellen, C. Linsmeier, A new high-throughput focused mev ion-beam analysis setup, Instruments 5 (1) (2021) 10, https://doi.org/10.3390/instruments5010010.

[16] M. Mayer, Simnra user's guide, 1997.

[17] R.L. Johnston, H.D. Holmgren, E.A. Wolicki, E.G. Illsley, Differential cross sections for the C12(He3, p)N14 reaction, Phys. Rev. 109 (3) (1958) 884–887, https://doi.org/10.1103/PhysRev.109.884.

[18] L. Csedreki, I. Uzonyi, G. Szíki, Z. Szikszai, G. Gyürky, Á. Kiss, Measurements and assessment of 12C(d,pγ)13C reaction cross sections in the deuteron energy range 740–2000kev for analytical applications, Nucl. Instrum. Methods Phys. Res., Sect. B, Beam Interact. Mater. Atoms 328 (2014) 59–64, https://doi.org/10.1016/j.nimb.2014.02.123.

[19] G. Terwagne, D.D. Cohen, G.A. Collins, Cross-section measurements of the 14n(3he,p)16o and 14n(3he,α)13n reactions between 1.6 and 2.8 mev, Nucl. Instrum. Methods Phys. Res., Sect. B, Beam Interact. Mater. Atoms 84 (4) (1994) 415–420, https://doi.org/10.1016/0168-583X(94)95335-X.

[20] M. Guitart Corominas, T. Schwarz-Selinger, Experimental determination of the 16o(3he,p0)18f differential cross section, Nucl. Instrum. Methods Phys. Res., Sect. B, Beam Interact. Mater. Atoms 450 (2019) 13–18, https://doi.org/10.1016/j.nimb.2018.05.018.

[21] A. Kreter, C. Brandt, A. Huber, S. Kraus, S. Möller, M. Reinhart, B. Schweer, G. Sergienko, B. Unterberg, Linear plasma device psi-2 for plasma-material interaction studies, Nucl. Fusion 68 (1) (2015) 8–14, https://doi.org/10.13182/FST14-906.

[22] M. Sackers, O. Marchuk, D. Dipti, Y. Ralchenko, S. Ertmer, S. Brezinsek, A. Kreter, Zeeman effect of isotopes of kr and xe investigated at the linear plasma device psi-2, Plasma Sources Sci. Technol. 33 (2) (2024) 025015, https://doi.org/10.1088/1361-6595/ad23fa.

[23] K. Schmid, M. Mayer, C. Adelhelm, M. Balden, S. Lindig, Impact of gyro-motion and sheath acceleration on the flux distribution on rough surfaces, Nucl. Fusion 50 (10) (2010) 105004, https://doi.org/10.1088/0029-5515/50/10/105004.

[24] H.Y. Xu, Y.B. Zhang, Y. Yuan, B.Q. Fu, A. Godfrey, G. de Temmerman, W. Liu, X. Huang, Observations of orientation dependence of surface morphology in tungsten implanted by low energy and high flux d plasma, J. Nucl. Mater. 443 (1–3) (2013) 452–457, https://doi.org/10.1016/j.jnucmat.2013.07.062.

[25] A. Eksaeva, E. Marenkov, D. Borodin, A. Kreter, M. Reinhart, A. Kirschner, J. Romazanov, A. Terra, S. Brezinsek, K. Nordlund, Ero modelling of tungsten erosion in the linear plasma device psi-2, Nucl. Mater. Energy 12 (2017) 253–260, https://doi.org/10.1016/j.nme.2017.03.014.

[26] R. Sakamoto, E. Bernard, A. Kreter, C. Martin, Impact of helium and hydrogen plasma exposure on surface damage and erosion of tungsten, Nucl. Fusion 64 (3) (2024) 036008, https://doi.org/10.1088/1741-4326/ad1fab.

[27] J. Schmitz, A. Litnovsky, F. Klein, T. Wegener, X.Y. Tan, M. Rasinski, A. Mutzke, P. Hansen, A. Kreter, A. Pospieszczyk, S. Möller, J.W. Coenen, C. Linsmeier, U. Breuer, J. Gonzalez-Julian, M. Bram, Wcry smart alloys as advanced plasma-facing materials – exposure to steady-state pure deuterium plasmas in psi-2, Nucl. Mater. Energy 15 (2018) 220–225, https://doi.org/10.1016/j.nme.2018.05.002.

[28] H.Y. Xu, G.N. Luo, H. Schut, Y. Yuan, B.Q. Fu, A. Godfrey, W. Liu, G. Temmerman, Enhanced modification of tungsten surface by nanostructure formation during high flux deuterium plasma exposure, J. Nucl. Mater. 447 (1–3) (2014) 22–27, https://doi.org/10.1016/j.jnucmat.2013.12.010.

[29] M. Reinhart, A. Kreter, L. Buzi, M. Rasinski, A. Pospieszczyk, B. Unterberg, C. Linsmeier, Influence of plasma impurities on the deuterium retention in tungsten exposed in the linear plasma generator psi-2, J. Nucl. Mater. 463 (2015) 1021–1024, https://doi.org/10.1016/j.jnucmat.2014.11.045.

[30] J. Schmitz, A.M. Litnovsky, F. Klein, X. Tan, U. Breuer, M. Rasinski, S. Ertmer, A. Kreter, J. Gonzalez-Julian, M. Bram, J.W. Coenen, C. Linsmeier, Argon-seeded plasma exposure and oxidation performance of tungsten-chromium-yttrium smart al-

loys, Tungsten 1 (2) (2019) 159–168, https://doi.org/10.1007/s42864-019-00016-7, https://link.springer.com/article/10.1007/s42864-019-00016-7.

[31] W. Eckstein, Calculated Sputtering, Reflection and Range Values, Max-Planck-Institut für Plasmaphysik, 2002.

[32] J. Romazanov, S. Brezinsek, D. Borodin, M. Groth, S. Wiesen, A. Kirschner, A. Huber, A. Widdowson, M. Airila, A. Eksaeva, I. Borodkina, C. Linsmeier, Beryllium global erosion and deposition at jet-ilw simulated with ero2.0, Nucl. Mater. Energy 18 (2019) 331–338, https://doi.org/10.1016/j.nme.2019.01.015.

[33] Y. Mao, J.W. Coenen, A. Terra, L. Gao, A. Kreter, M. Wirtz, C. Liu, C. Chen, J. Riesch, Y. Wu, C. Broeckmann, C. Linsmeier, Demonstrating tungsten fiber-reinforced porous-matrix tungsten composites for future fusion application, Nucl. Fusion 62 (10) (2022) 106029, https://doi.org/10.1088/1741-4326/ac8c55.

[34] H. Tu, S. Wang, L. Cui, L. Cheng, G.-H. Lu, D.J. O'Connor, L. Shi, The influence of impurities on the erosion of tungsten by low energy high flux deuterium plasma irradiation, J. Nucl. Mater. 556 (2021) 153168, https://doi.org/10.1016/j.jnucmat.2021.153168.

[35] T.H. Kwon, S. Park, J.M. Ha, Y.-S. Youn, Study on sputtering yield of tungsten with different particle sizes: surface roughness dependence, Nucl. Eng. Technol. 53 (6) (2021) 1939–1941, https://doi.org/10.1016/j.net.2020.12.024.

[36] C. Cupak, P.S. Szabo, H. Biber, R. Stadlmayr, C. Grave, M. Fellinger, J. Brötzner, R.A. Wilhelm, W. Möller, A. Mutzke, M.V. Moro, F. Aumayr, Sputter yields of rough surfaces: importance of the mean surface inclination angle from nano- to microscopic rough regimes, Appl. Surf. Sci. 570 (2021) 151204, https://doi.org/10.1016/j.apsusc.2021.151204.

[37] K. Schlueter, K. Nordlund, G. Hobler, M. Balden, F. Granberg, O. Flinck, T.F. Da Silva, R. Neu, Absence of a crystal direction regime in which sputtering corresponds to amorphous material, Phys. Rev. Lett. 125 (22) (2020) 225502, https://doi.org/10.1103/PhysRevLett.125.225502.

[38] M. Reza, Z. Sajuri, J. Yunas, J. Syarif, Effect of sputtering target's grain size on the sputtering yield, particle size and coercivity (hc) of ni and ni20al thin films, IOP Conf. Ser., Mater. Sci. Eng. 114 (2016) 012116, https://doi.org/10.1088/1757-899X/114/1/012116.

[39] R.K. Khisamov, N.N. Andrianova, A.M. Borisov, M.A. Ovchinnikov, R.R. Mulyukov, Effect of grain size and texture of polycrystalline tungsten on its ion-beam sputtering, Surf. Investig.: X-Ray Synchrotron Neutron Tech. 19 (1) (2025) 179–189, https://doi.org/10.1134/S1027451025700284.

[40] S. Wang, W. Guo, L. Cheng, T. Schwarz-Selinger, M. Liu, X. Zhu, Y. Yuan, E. Fu, L. Guang-Hong, Dependence of blistering and deuterium retention on damage depth in damaged tungsten exposed to deuterium plasma, Nucl. Fusion 61 (5) (2021) 056003, https://doi.org/10.1088/1741-4326/abecca.

[41] S. Ryabtsev, Y. Gasparyan, M. Zibrov, A. Shubina, A. Pisarev, Deuterium thermal desorption from vacancy clusters in tungsten, Nucl. Instrum. Methods Phys. Res., Sect. B, Beam Interact. Mater. Atoms 382 (2016) 101–104, https://doi.org/10.1016/j.nimb.2016.04.038.

[42] A.V. Golubeva, V.A. Kurnaev, M. Mayer, J. Roth, Hydrogen retention in plasma-sprayed tungsten, in: AIP Conference Proceedings, AIP, 2006, pp. 12–21.

[43] V. Alimov, B. Tyburska, O.V. Ogorodnikova, J. Roth, K. Isobe, T. Yamanishi, Deuterium retention in porous vacuum plasma-sprayed tungsten coating exposed to low-energy, high-flux pure and helium-seeded d plasmas, J. Nucl. Mater. 415 (1) (2011) S628–S631, https://doi.org/10.1016/j.jnucmat.2010.08.054, https://www.sciencedirect.com/science/article/pii/S0022311510004459.

[44] O.V. Ogorodnikova, K. Sugiyama, T. Schwarz-Selinger, T. Dürbeck, M. Balden, Ion-induced deuterium retention in tungsten coatings on carbon substrate, J. Nucl. Mater. 419 (1–3) (2011) 194–200, https://doi.org/10.1016/j.jnucmat.2011.07.023.

[45] V. Alimov, W.M. Shu, J. Roth, S. Lindig, M. Balden, K. Isobe, T. Yamanishi, Temperature dependence of surface topography and deuterium retention in tungsten exposed to low-energy, high-flux d plasma, J. Nucl. Mater. 417 (1–3) (2011) 572–575, https://doi.org/10.1016/j.jnucmat.2011.01.088.

[46] M. Balden, A. Manhard, S. Elgeti, Deuterium retention and morphological modifications of the surface in five grades of tungsten after deuterium plasma exposure, J. Nucl. Mater. 452 (1–3) (2014) 248–256, https://doi.org/10.1016/j.jnucmat.2014.05.018.

[47] Y. Hatano, M. Shimada, T. Otsuka, Y. Oya, V. Alimov, M. Hara, J. Shi, M. Kobayashi, T. Oda, G. Cao, K. Okuno, T. Tanaka, K. Sugiyama, J. Roth, B. Tyburska-Püschel, J. Dorner, N. Yoshida, N. Futagami, H. Watanabe, M. Hatakeyama, H. Kurishita, M. Sokolov, Y. Katoh, Deuterium trapping at defects created with neutron and ion irradiations in tungsten, Nucl. Fusion 53 (7) (2013) 073006, https://doi.org/10.1088/0029-5515/53/7/073006.

[48] M. Shimada, G. Cao, Y. Hatano, T. Oda, Y. Oya, M. Hara, P. Calderoni, The deuterium depth profile in neutron-irradiated tungsten exposed to plasma, Phys. Scr. T 145 (2011) 014051, https://doi.org/10.1088/0031-8949/2011/t145/014051.

[49] K. Sugiyama, K. Krieger, M. Mayer, S. Lindig, M. Balden, T. Dürbeck, Deuterium retention in bulk tungsten exposed to the outer divertor plasma of asdex upgrade, Phys. Scr. T 145 (2011) 014033, https://doi.org/10.1088/0031-8949/2011/t145/014033.

[50] A. Kreter, D. Nishijima, R.P. Doerner, M. Freisinger, C. Linsmeier, Y. Martynova, S. Möller, M. Rasinski, M. Reinhart, A. Terra, Y. Torikai, B. Unterberg, Influence of plasma impurities on the fuel retention in tungsten, Nucl. Fusion 59 (8) (2019) 086029, https://doi.org/10.1088/1741-4326/ab235d.

[51] J. Roth, K. Schmid, Hydrogen in tungsten as plasma-facing material, Phys. Scr. T 145 (2011) 014031, https://doi.org/10.1088/0031-8949/2011/T145/014031.

[52] C. García-Rosales, P. Franzen, H. Plank, J. Roth, E. Gauthier, Re-emission and thermal desorption of deuterium from plasma sprayed tungsten coatings for application in asdex-upgrade, J. Nucl. Mater. 233–237 (1996) 803–808, https://doi.org/10.1016/S0022-3115(96)00185-7.

[53] O.V. Ogorodnikova, J. Roth, M. Mayer, Ion-driven deuterium retention in tungsten, J. Appl. Phys. 103 (3) (2008), https://doi.org/10.1063/1.2828139.

[54] A. Pundt, S. Wagner, Hydrogen interactions with defects in materials, Chem. Ing. Tech. 96 (1–2) (2024) 182–191, https://doi.org/10.1002/cite.202300235.

[55] M.L. Martin, P. Sofronis, Hydrogen-induced cracking and blistering in steels: a review, J. Nat. Gas Sci. Eng. 101 (2022) 104547, https://doi.org/10.1016/j.jngse.2022.104547.

[56] Q. Yu, M.J. Simmonds, R. Doerner, G.R. Tynan, L. Yang, B.D. Wirth, J. Marian, Understanding hydrogen retention in damaged tungsten using experimentally-guided models of complex multispecies evolution, Nucl. Fusion 60 (9) (2020) 096003, https://doi.org/10.1088/1741-4326/ab9b3c.

[57] H.-B. Zhou, Y.-L. Liu, S. Jin, Y. Zhang, G.-N. Luo, G.-H. Lu, Investigating behaviours of hydrogen in a tungsten grain boundary by first principles: from dissolution and diffusion to a trapping mechanism, Nucl. Fusion 50 (2) (2010) 025016, https://doi.org/10.1088/0029-5515/50/2/025016.

[58] T. Tanabe, Review of hydrogen retention in tungsten, Phys. Scr. T 159 (2014) 014044, https://doi.org/10.1088/0031-8949/2014/T159/014044.

[59] A. Manhard, K. Schmid, M. Balden, W. Jacob, Influence of the microstructure on the deuterium retention in tungsten, J. Nucl. Mater. 415 (1) (2011) S632–S635, https://doi.org/10.1016/j.jnucmat.2010.10.045.

[60] V. Alimov, B. Scherzer, Deuterium retention and re-emission from tungsten materials, J. Nucl. Mater. 240 (1) (1996) 75–80, https://doi.org/10.1016/S0022-3115(96)00442-4.